The International Journal of Advanced Manufacturing Technology (2018) 96:2725–2733
https://doi.org/10.1007/s00170-018-1773-8

ORIGINAL ARTICLE

Surface quality monitoring based on time-frequency features of acoustic emission signals in end milling Inconel-718

Zhimeng Li[1] · Guofeng Wang[1] · Gaiyun He[1]

Received: 16 October 2017 / Accepted: 11 February 2018 / Published online: 24 February 2018

Abstract
Surface quality deterioration is prone to be found in Inconel-718 milling process, which leads to the decrease of fatigue life of aerospace critical safety components. Therefore, in-process detection of surface quality plays an important role in guaranteeing the workpiece quality and improving the production efficiency. In this paper, a surface quality monitoring system based on time-frequency features of acoustic emission signals is established. The main characteristic of this system is that a two-step recognition is performed through the binary clustering to realize the monitoring of surface roughness and the precise recognition of the surface defects, respectively. A new feature extraction method by means of the normalized time-frequency matrix is proposed to obtain the sensitive information of surface quality. In addition, to accomplish the clustering automatically, the improved method of clustering by fast search and find of density peaks is utilized. The experimental verification with different cutting depth is designed to test the effectiveness of the system. Validation results show that the accuracy of the two steps are 99 and 72%, respectively.

Keywords Surface quality · Time-frequency analyze · Feature extraction · Acoustic emission · Clustering

1 Introduction

Inconel-718 is widely used in critical components of the hot section of aerospace engines, such as blades, combustion chamber wall, vectoring nozzle, etc. However, due to the undesirable properties such as the difficulty in cutting at elevated temperatures, work hardening nature, and low thermal conductivity of Inconel-718, it is prone to causing tool wear during milling process. Thus, the desirable surface quality is difficult to be guaranteed. In fact, the surface roughness and surface damages are two main concerned aspects of surface quality in the milling process of Inconel-718 [1] and their degradation leads to an obvious decrease in the fatigue performances of the parts [2]. Therefore, it is of great significance to monitor the surface quality in the cutting process of Inconel-718.

To date, the key aspect of surface quality is surface topography which mainly includes surface roughness and surface defects [3]. Most studies achieved surface roughness monitoring through the analysis of the signals including cutting force, vibration, and acoustic emission in the cutting process. Zeng [4] and Ren [5] realized the monitoring of tool conditions and demonstrated the effect of tool wear on the surface roughness. The research by Pawade et al. [6] showed that the larger cutting forces generated poorer surface finish as well as extensive surface damages. Somkiat et al. [7] presented a model developed for the prediction of surface roughness through analyzing the relationship with cutting force and cutting temperature. Besides the cutting force, Khorasani [8] and Quintana [9] modeling the vibration signals to achieve surface roughness monitoring. Plaza and López [10, 11] applied wavelet packet transform method for feature extraction of vibration signals, which enabled the monitoring of surface roughness. Huang et al. [12] proposed a Grey online modeling surface roughness monitoring system which required less data and no training time. In addition, the relationship between AE and surface roughness was studied by Beggan [13]. In contrast with the surface roughness, several researches focus on the monitoring of surface defects. Pawade and Joshi [14] found that the surface generation mechanism can be assessed in terms of the

✉ Guofeng Wang
gfwangmail@tju.edu.cn

[1] Tianjin Key Laboratory of Equipment Design and Manufacturing Technology, Tianjin University, Tianjin 300072, China

energy, number of counts, and mean frequency amplitude of the AE signals. Accordingly, the AE energy profiles with more perturbations were used to indicate severe surface alterations or defects. Axinte [15] attempted to correlate the quality of the machined surface and the output signals namely acoustic emission, vibration, and cutting forces during broaching. The acoustic emission signals proved to be efficient for the detection of small surface anomalies. Marinescu et al. [16, 17] proposed a method of time-frequency analysis of AE signals to monitor the surface defects caused by damaged cutting edge. The above researches implemented the diagnosis of surface quality through the recognition of single factor such as surface roughness and surface defects. However, both the surface roughness and the surface defects are the crucial issues that usually need to be monitored simultaneously [18, 19]. Therefore, the surface quality monitoring system including the two aspects above needs to be established.

In this paper, the surface quality monitoring system based on time-frequency analysis of AE signals is established to realize the monitoring of surface roughness and identification of surface defect. In order to find the spectral information sensitive to the surface quality, the new feature extraction method based on normalized time-frequency matrix is proposed. The improved method of clustering by fast search and find of density peaks (CFSFDP) is utilized in a two-step identification by which the workpiece surfaces are divided into three types according to the degree of deterioration.

The remainder of this paper is organized as follows: in Section 2, methodologies of the study are presented and the proposed normalized time-frequency matrix and improved CFSFDP are defined. In Section 3, experimental setup is illustrated and accurate matching of the field emission scanning electron microscope images and the AE signals is presented. In Section 4, the feature pool is built based on the time-frequency method and the optimal feature sets are selected using the ratio of between-class scatter and within-class scatter. With the selected features, the recognition of the surface roughness and the surface defects is realized through the improved CFSFDP. Some useful conclusions are given in the last section.

2 Methodologies of the study

2.1 Normalized time-frequency feature extraction

The time-frequency matrix (TFM) is obtained after performing time-frequency transform on the AE signals and it reflects the energy distribution of the signals over a time-frequency two-dimensional plane. However, the spectral information independent of energy cannot be reflected by TFM. Therefore, a method of normalizing the TFM along the frequency direction is proposed, which can eliminate the effect of the changing AE energy. The normalization of TFM is achieved by the following formula:

$$p[n] = P[n] - \frac{\sum_{k=1}^{M}[n,k]}{M} \tag{1}$$

where $P[n, k]$ is the TFM with N columns and M rows, and p is the normalized time-frequency matrix (NTFM) which can reflect the variation of the spectral information independent of energy.

2.2 Improved clustering by fast search and find of density peaks

CFSFDP is a clustering method based on both partition and density, proposed by Alex Rodriguez and Alessandro Laio [20]. The main disadvantage of the original algorithm is that the clustering centers can only be determined by manual selection. Therefore an improved CFSFDP is made to realize clustering automatically (see Fig. 1). Firstly, the distance matrix D containing the distances between each pair of the data points is calculated as the similarity measure. Secondly, the density and distance of each data point are calculated to construct the decision graph. For data point i, the density is defined as the number of points that are closer than dc to it, which can be calculated as:

$$\rho_i = \sum_j \chi\left(d_{ij} - d_c\right) \tag{2}$$

where dc is the value that makes the average density of the entire data equal to 1 to 2% of the data capacity. Then, the distance δ from each data point to the point with higher density is calculated as follows:

$$\delta_i = \min_{j:\rho_j > \rho_i}\left(d_{ij}\right) \tag{3}$$

If the number of points with higher density is more than one, the minimum distance is chosen. Thirdly, in order to identify the cluster center automatically, a value S is proposed to measure the weight of each point as the candidate of cluster centers, which can be calculated as:

$$S_i = \rho_i \times \delta_i \tag{4}$$

Since the issue in this article is a binary classification problem, data points with the first and the second large S are defined as the cluster centers. Finally, based on the principle of density clustering, the remaining data points are divided into several categories.

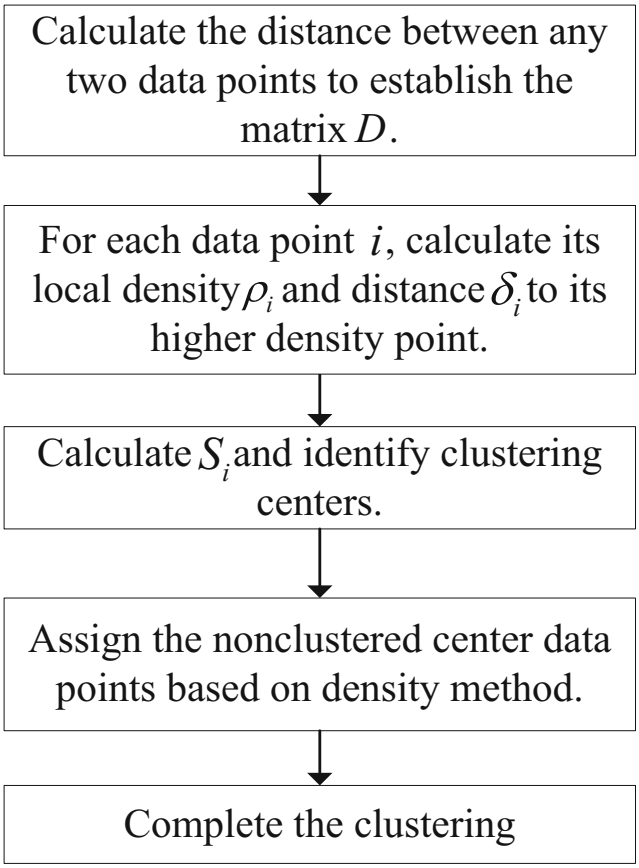

Fig. 1 Flowchart of the improved CFSFDP

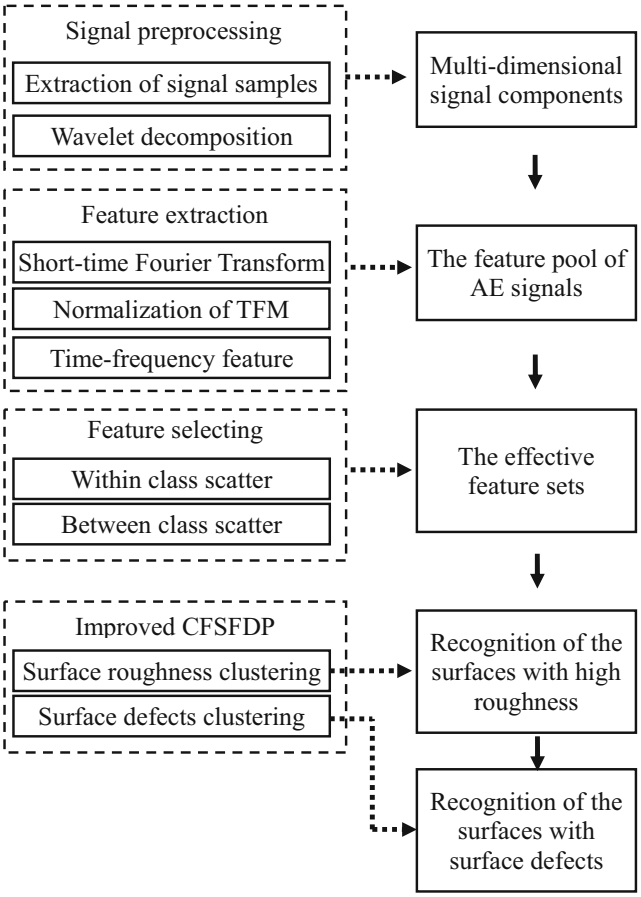

Fig. 2 Framework of the two-step recognition

2.3 Framework of the two-step recognition

To accomplish the two-step recognition of the surface quality, the whole monitoring system is given in Fig. 2. The raw AE signals are processed using the signal preprocessing, feature extraction, and feature selecting by which the information reflect the surface quality are obtained. In the signal preprocessing stage, the AE signals are preprocessed to obtain multi-dimensional signal components using the discrete wavelet transform. Then the feature extraction based on time-frequency method is performed using the Short-time Fourier Transform and NTFM is utilized to find the spectral information of AE signals. Accordingly, the time-frequency features are extracted and the feature pool of AE signals is established correspondingly. In order to find the effective feature set sensitive to surface quality, the indicators based on within-class scatter and between-class scatter are used and two effective feature sets corresponding to the surface roughness and the surface defects are constructed, respectively. Based on the selected feature sets, the two-step identification of surface roughness and surface defects is achieved by the improved CFSFDP algorithm. In the first step, the surfaces with high roughness are recognized to separate them from the normal surfaces which are free of defects. In the second step, the high roughness surfaces are further divided into the surfaces with and without defects. Finally, the recognition of three types of surfaces is realized to achieve the detailed monitoring of surface quality.

3 Experimental setup

The experimental setup was designed as shown in Fig. 3. The workpiece material used in milling test was Nickel 718 and its properties are listed in Table 1. A PVD coated end milling cutter with 25 mm diameter (APMT1135PDER-H2 VP15TF) was utilized and the corresponding experiment was realized using Hanland xk714d three-axis vertical machining center.

The AE sensor used was a wideband piezoelectric sensor with a response frequency of 10 kHz to 1 MHz and it was mounted under the workpiece to minimize the attenuation of the AE signals. A high sample rate DAQ was used to collect the AE signals with the sampling frequency of 6 MHz, so that each AE waveform in the cutting process could be depicted by at least 6 data points, ensuring an accurate AE waveform analysis. When the machining was finished, the workpiece surface was observed to get the surface quality information by field emission scanning electron microscope and optical microscopy with large depth of field, respectively. Finally,

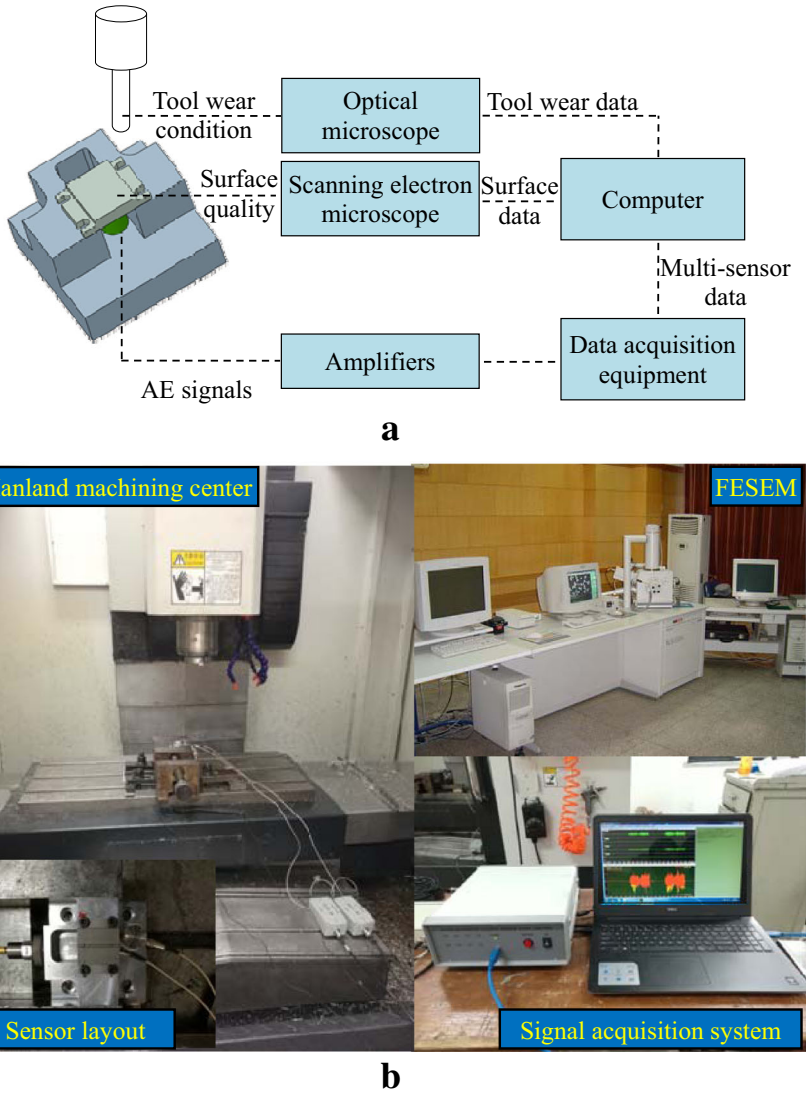

Fig. 3 Experimental setup. **a** Dataflow of the monitoring system. **b** Experimental setup

the entire information including the cutting condition parameters, the machining surface quality, and the corresponding AE signals was established.

Cutting parameters were given in Table 2, in which the spindle speed was 500 r/min and the feed speed was 0.1 mm/tooth. In order to verify the AE features proposed in this paper, a new insert as well as a breakage insert were utilized to produce milling surfaces with different roughness and defects, which were named as T1 and T2, respectively. The cutting depth was set to 0.1 and 0.2 mm which were called Path 1 and Path 2 with 30 mm cutting length. Path 1 was used to establish the optimal feature sets through the time-frequency feature extraction and feature selection based on class scatter. Path 2 was the verification experiment to test the effectiveness of the selected feature sets and the performance of the whole monitoring system.

Table 1 Properties of Nickel 718

Properties	Value
Melting temperature (°C)	1260–1320
Density (g/cm^3)	8.24
Thermal conductivity (W/mK)	21.2
Tensile strength (Rm N/mm^2)	965
Yield strength (Rp0.2 N/mm^2)	550
Brinell hardness (HB)	363

Table 2 Cutting parameters used for experimental trials

Variable factors	Levels
Cutting speed, v_c [m/min]	39.25
Feed rate, f [mm/rev]	0.1
Width of cut, ae [mm]	1
Depth of cut, ap [mm]	0.1 (Path 1), 0.2 (Path 2)
Coolant	Dry

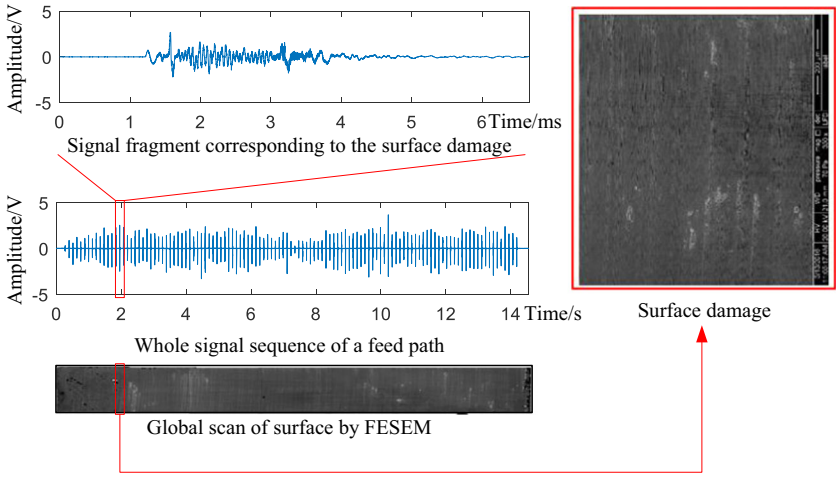

Fig. 4 Methodology for pinpointing the special signals of surface damages

In order to achieve accurate matching of the FESEM images and the AE signals during the cutting process, the cutting width was designed to be 1 mm. The FESEM images of the finished workpiece surface were exactly spliced together to obtain the high-resolution image of the whole workpiece surface, as shown in Fig. 4. The rotation angle corresponding to each cutting is 5° so that the adjacent two cutting AE signals can be well separated. Through the above experimental setup, the single piece of AE signal matched with the workpiece surface of each tooth in the cutting process was obtained, which make it possible to monitor the surface defects.

4 Results and discussions

4.1 Feature extraction and selection

4.1.1 Time-frequency feature extraction

The milled surfaces formed by the new cutter (T1) and breakage cutter (T2) are presented in Fig. 5, respectively. Under the optical microscope, it can be observed from Fig. 5a–d that the surface formed by T1 is almost free of abnormality while the surface formed by T2 has a large area of surface abnormality. Further measurement shows that the surface roughness of Path 1 and Path 2 was 0.113 and 0.148 μm, respectively, if T1 was used and they increase to 0.545 and 0.458 μm, respectively, if T2 was utilized, which demonstrates that tool wear deteriorates the surface roughness obviously. To analyze the surface quality deeply, field emission scanning electron microscope was used to observe the formed surface of T1 and T2 cutter. It can be found that there is almost no surface defect in the surface formed by T1 while there are many defects that can be observed in the surface formed by T2. Moreover, the appearance of surface defect under Path 1 and Path 2 is random because of the uniformity of the cutting zone and the carbide particle in the material (Fig. 5e–i). These results prove that the surface roughness and the surface defects are two different surface deterioration phenomena although they are all caused by tool wear.

To realize the accurate recognition of the surface roughness and surface defects, the time-frequency features of AE signals

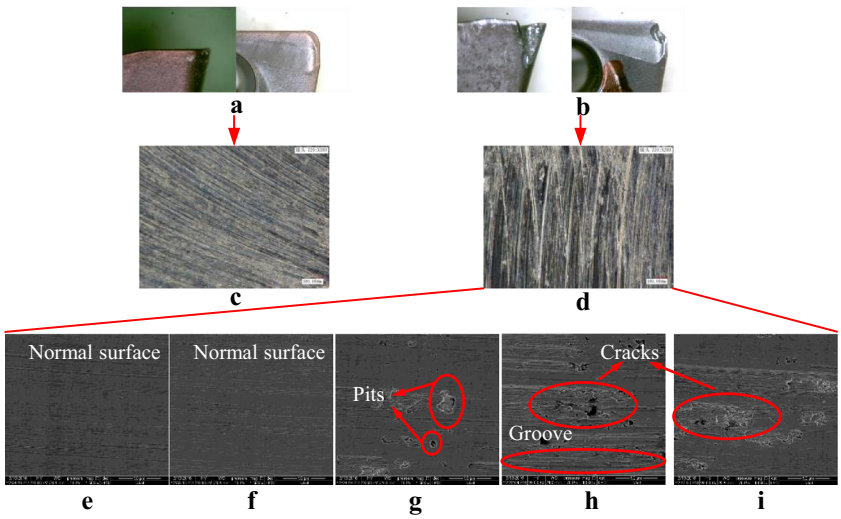

Fig. 5 Surface quality corresponding to the tool condition. **a** New cutting insert; **b** breakage cutting insert; **c**, **d** surface observed via optical microscope; **e**–**i** surface observed via FESEM

Table 3 List of the selected features

Feature	Mathematical expression	Feature	Mathematical expression
Band energy	$EB_{(t,f)} = \sum_{k=(i-1)\Delta+1}^{[i\Delta]} P[n,k]$	Total energy	$E_{(t,f)} = \sum_{n=1}^{N}\sum_{k=1}^{M} P[n,k]$
Variance along time direction	$\hat{\sigma}_t^2 = \mathrm{var}(P_t[\mathrm{n}])$	Variance along frequency direction	$\hat{\sigma}_f^2 = \mathrm{var}(P_f[\mathrm{k}])$
Skewness along time direction	$\hat{\gamma}_t = \mathrm{ske}(P_t[\mathrm{n}])$	Skewness along frequency direction	$\hat{\gamma}_f = \mathrm{ske}(P_f[\mathrm{k}])$
Kurtosis along time direction	$\hat{\kappa}_t = \mathrm{kur}(P_t[\mathrm{n}])$	Kurtosis along frequency direction	$\hat{\kappa}_f = \mathrm{kur}(P_f[\mathrm{k}])$
Frequency corresponds to the maximum power	$\hat{f}_{P_{f\max}} = F(\lfloor P_{f\max} \rfloor)$	Weighted mean value along frequency direction	$\hat{f}_m = \frac{\sum_k F[k]P_f[k]}{M}$

The operational symbols var, ske, and kur are used to represent the functions of variance, skewness, and kurtosis, respectively. The operational symbol $\lfloor \bullet \rfloor$ means the operation of extracting the subscript index of the object in the square brackets

corresponding to the surface formed by each tooth are extracted as follows: At first, the milled surfaces coming from the cutting process of T1 and T2 are extracted respectively with 5 mm length, which corresponds to 50 pieces of AE signals. The AE signals corresponding to the surfaces of T2 are further divided into two classes where the first class with surface defects has 20 samples and the second class without surface defects has 30 samples. Secondly, for each piece of AE signal, the feature extraction is performed to construct the feature pool using the method of Fig. 1. In order to separate the noise originating from the vibration of tool workpiece system and the environmental disturb, the AE signal was decomposed by using Discrete Wavelet Transform and Short-Time Fourier Transform (STFT) is further utilized to analyze the signal components corresponding to the high frequency band. Furthermore, the TFM and the NTFM are obtained from which the time-frequency features are extracted. All the features are listed in Table 3, where $P_t[n]$ and $P_f[k]$ are the vectors obtained by the summation of $P[n,k]$ in time domain and frequency domain, respectively, $F[k]$ is the vector of frequencies corresponding to each column of matrix $P[n,k]$.

4.1.2 The optimal feature sets sensitive to the surface quality

In order to demonstrate the effectiveness of the feature extraction method in this paper, the conventional AE features in [5] are also extracted from each of the wavelet components. The features are the average value (AE_{AV}), the RMS value (AE_{RMS}), the standard deviation (AE_{SD}), the maximum value (AE_{MX}), the minimum value (AE_{MI}), the range (AE_{RG}), the maximum minus average (AE_{MX-AV}), and the minimum minus average (AE_{MI-AV}), respectively. To find the optimal feature sets, the effectiveness of all the above features are evaluated via the ratio of between-class scatter and within-class scatter:

$$S = \frac{S_B}{S_W} \tag{5}$$

where the between-class scatter is calculated by the following equation:

$$S_B = \frac{1}{2}\sum_{i=1}^{M} P(\Omega_i)\sum_{j=1}^{M} P(\Omega_j) S_B^{(ij)} \tag{6}$$

Ω_i is the sample set of the ith class. The greater the between-class scatter, the better the validity of the feature. The within-class scatter is calculated as follows:

$$S_W = \sum_{i=1}^{M} P(\Omega_i) S_W^{(i)} \tag{7}$$

The smaller the within-class scatter, the better the validity of the feature.

Through feature selection using the above scatter index, it can be shown that different features are sensitive to surface roughness and surface defects, respectively. The two most effective features to characterize the surface roughness are both from the first wavelet component of the AE signal, which is called the variance and skewness of NTFM along the time direction. Meanwhile, the two most effective features to characterize the surface defects are called the weighted mean frequency and the frequency peak of TFM from the fourth wavelet component. The results are listed in Table 4.

Table 4 Optimal feature set under different criterion

Surface roughness		Surface defects	
Specific meaning of features	Validity	Specific meaning of features	Validity
The variance of NTFM energy along the time direction from the first wavelet component	0.451	The weighted mean frequency of TFM from the fourth wavelet component	0.213
The skewness of NTFM energy along the time direction from the first wavelet component	0.384	The frequency peak of TFM from the fourth wavelet component	0.275

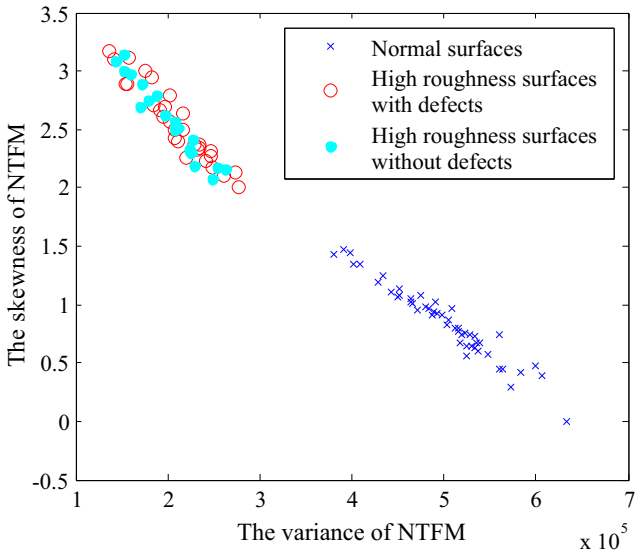

Fig. 6 Spatial distribution of optimal feature vectors to surface roughness

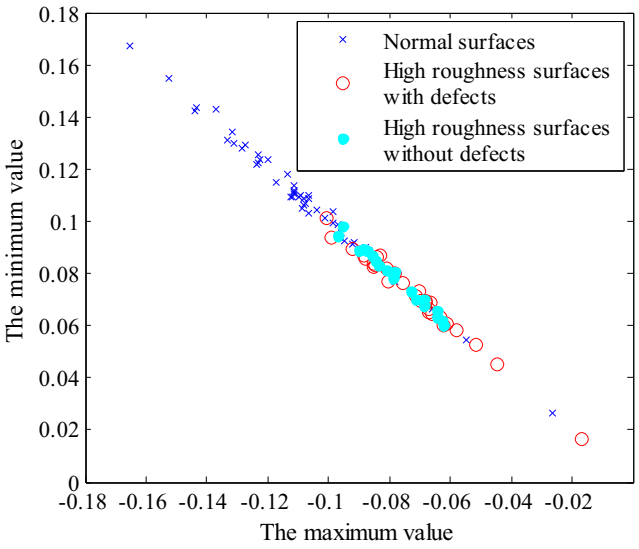

Fig. 8 Spatial distribution of conventional AE features to surface roughness

In order to demonstrate the effectiveness of optimal feature sets obviously, the spatial distribution of feature vectors for the surface roughness and the surface defects are demonstrated, respectively (see Fig. 6 and Fig. 7). It can be seen from Fig. 6 that the surfaces of T1 and T2 are completely separated, where the surfaces with high roughness value have the higher skewness and lower variance than the normal surfaces. However, the high roughness surfaces with and without defects cannot be distinguished these two features. Therefore, the other two features are used and a good separation between the surfaces with and without defects could be found in Fig. 7, where the surface defects have higher average frequency and its peak. In order to realize comparison, the conventional AE features which have the high ratio S are also used to construct the spatial distribution. Results show that the two most effective features to characterize the surface roughness are AE_{MX} and AE_{MI} from the fourth wavelet component with validity values of 0.123 and 0.124, respectively. The two most effective features to characterize the surface defects are AE_{MX} and AE_{MI} from the fifth wavelet component with validity values of 0.155 and 0.154, respectively. However, the conventional AE features cannot provide desirable separation for both surface roughness and surface defects, as depicted in Figs. 8 and 9.

4.2 Clustering results and performance evaluation

To realize the pattern recognition of three types of surfaces above, the two-step binary clustering by improved CFSFDP is performed on the obtained optimal feature sets. In the process

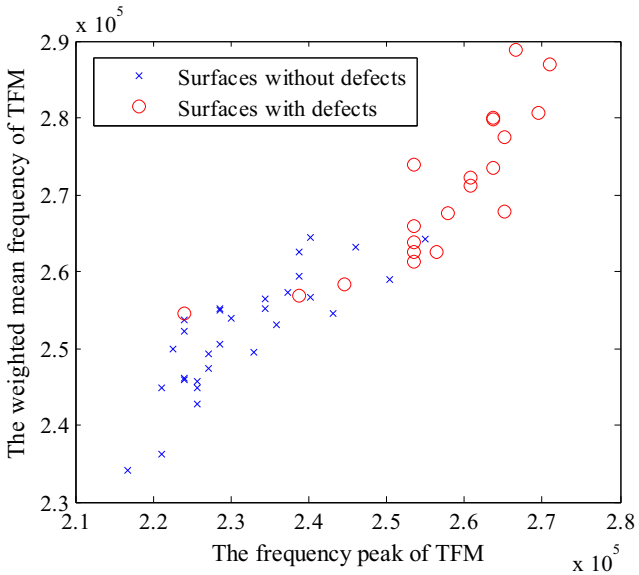

Fig. 7 Spatial distribution of optimal feature vectors to surface defects

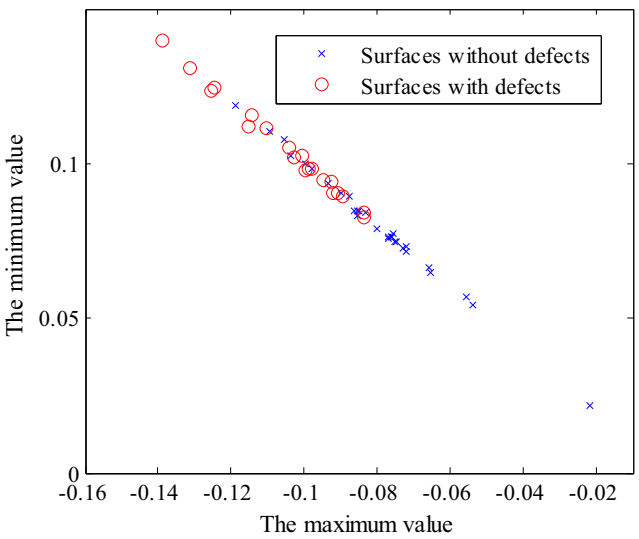

Fig. 9 Spatial distribution of conventional AE features to surface defects

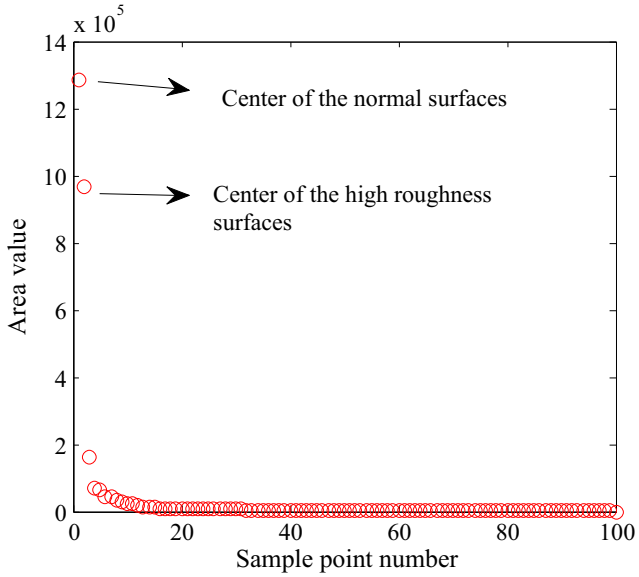

Fig. 10 Area values of data points for surface roughness clustering

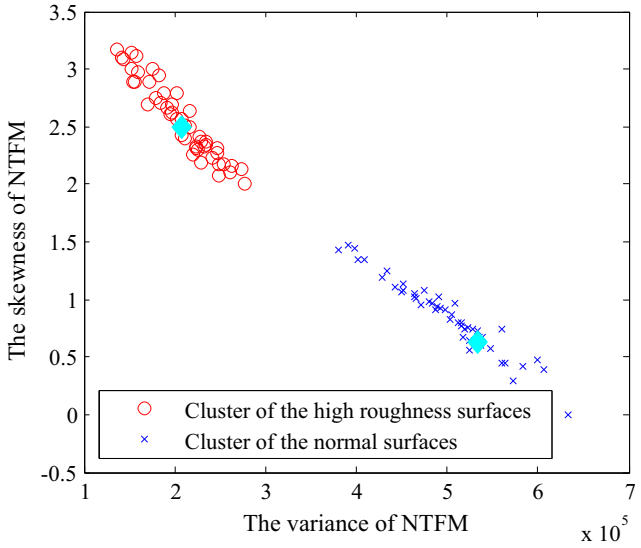

Fig. 12 Clustering result of surface roughness

of the original CFSFDP, the clustering centers could only be manually determined. In this paper, the improved CFSFDP is proposed to automatically determine the clustering centers by selecting the two points with the largest area value (illustrated in Fig. 10 and Fig. 11). Subsequently, the remaining data points can be assigned to its cluster by finding its nearest neighbor of higher density. The clustering results in the two steps for surface roughness and surface defects are presented in Figs. 12 and 13 where two big points with bright color denote the clustering centers. Then the performance *ERR* is utilized to evaluate the effectiveness of the clustering results, which can be calculated as [21]:

$$ERR = 1 - \frac{\sum_{i=1}^{n} \delta\left(C_i^a, map\left(C_i^u\right)\right)}{n} \tag{8}$$

where C_i^a and C_i^u are the class label and cluster label, respectively. $\delta(a, b)$ is the function that equals 1 if $a = b$ and equals 0 otherwise. map(•) is the permutation function that maps each cluster label to a class label. The lower *ERR* demonstrates the better clustering result. Results show that the accuracy of the two steps is 100 and 74%, respectively.

In order to test the effectiveness of the whole monitoring system proposed in this paper, the same process was performed on the Path 2 as experimental verification and the recognition results are listed in Table 5. It is obviously that both the clustering accuracies of monitoring surface

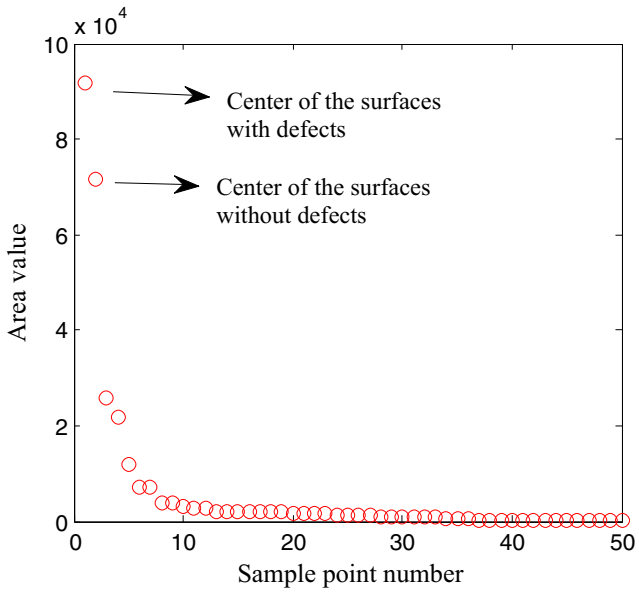

Fig. 11 Area values of data points for surface defects clustering

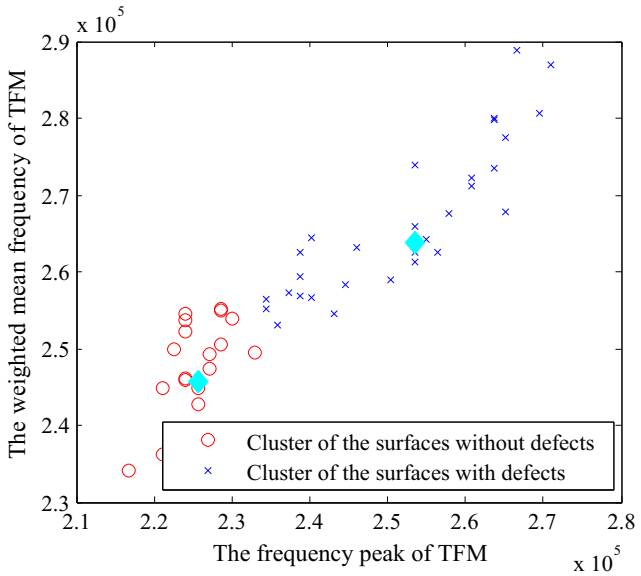

Fig. 13 Clustering result of surface defects

Table 5 Clustering accuracy (%)

Clustering objective	Path 1	Path 2
Surface roughness	100	99
Surface defects	74	72

roughness and surface defects were close to those of Path 1, indicating that the monitoring system was effective. However, compared with the high accuracy of monitoring surface roughness, the clustering accuracy for the surface defects was lower, which can be attributed to the complexity factors that cause the surface defects. Further research will be promoted to increase the accuracy of monitoring surface defects.

5 Conclusions

In this paper, an in-process detection system based on time-frequency analysis of AE signals is established to monitor the surface quality through two steps. The main advantage of the system is that the new feature extraction method based on NTFM is utilized. Accordingly, the optimal feature sets sensitive to the surface quality are obtained which provide better performance than the conventional AE features. In addition, a two-step recognition based on the binary clustering is performed to realize the monitoring of surface roughness and surface defects, respectively. Results show that the clustering accuracy of the two steps is 100 and 74%, respectively. To test the effectiveness of the proposed method, the experimental verification with different cutting depth is designed and the clustering accuracy of surface roughness and surface defects could be up to 99 and 72%, respectively.

Funding information This project is supported by the National Natural Science Foundation of China (51675369), Tianjin Science and Technology Program (16PTSYJC00150), National Natural Science Foundation of China (51420105007), and National Science and Technology Major Projects (2014ZX04012014).

References

1. Zhou JM, Bushlya V, Stahl JE (2012) An investigation of surface damage in the high speed turning of Inconel 718 with use of whisker reinforced ceramic tools. J Mater Process Technol 212(2):372–384
2. Huang Q, Ren JX (1991) Surface integrity and its effects on the fatigue life of the nickel-based superalloy GH33A. Int J Fatigue 13(4):322–326
3. Thakur A, Gangopadhyay S (2016) State-of-the-art in surface integrity in machining of nickel-based super alloys. Int J Mach Tool Manu 100:25–54
4. Zeng W, Jiang X, Blunt L (2009) Surface characterisation-based tool wear monitoring in peripheral milling. Int J Adv Manuf Technol 40(3–4):226–233
5. Ren Q, Balazinski M, Baron L et al (2014) Type-2 fuzzy tool condition monitoring system based on acoustic emission in micromilling. Inf Sci 255(1):121–134
6. Pawade RS, Joshi SS, Brahmankar PK et al (2007) An investigation of cutting forces and surface damage in high-speed turning of Inconel 718. J Mater Process Technol 192–193(10):139–146
7. Somkiat T, Somchart A, Sirichan T (2010) In-process monitoring and prediction of surface roughness on CNC turning by using response surface analysis. In: Hinduja S., Li L (eds) Proceedings of the 36th International MATADOR Conference. Springer, London, 2010:213-216. DOI: https://doi.org/10.1007/978-1-84996-432-6_49
8. Khorasani A, Yazdi MRS (2017) Development of a dynamic surface roughness monitoring system based on artificial neural networks (ANN) in milling operation. Int J Adv Manuf Technol 93:141–151
9. Quintana G, Garcia-Romeu ML, Ciurana J (2011) Surface roughness monitoring application based on artificial neural networks for ball-end milling operations. J Intell Manuf 22(4):607–617
10. Plaza EG, López PJN (2018) Application of the wavelet packet transform to vibration signals for surface roughness monitoring in CNC turning operations. Mech Syst Signal Process 98:902–919
11. Plaza EG, López PJN (2018) Analysis of cutting force signals by wavelet packet transform for surface roughness monitoring in CNC turning. Mech Syst Signal Process 98:634–651
12. Huang PB, Zhang HJ, Lin YC (2017) Development of a Grey online modeling surface roughness monitoring system in end milling operations. J Intell Manuf. https://doi.org/10.1007/s10845-017-1361-z
13. Beggan C, Woulfe M, Young P, Byrne G (1999) Using acoustic emission to predict surface quality. Int J Adv Manuf Technol 15(10):737–742
14. Pawade RS, Joshi SS (2012) Analysis of acoustic emission signals and surface integrity in the high-speed turning of Inconel 718. Proc Inst Mech Eng B J Eng 226(1):3–27
15. Axinte D (2004) Process monitoring to assist the workpiece surface quality in machining. Int J Mach Tool Manu 44(10):1091–1108
16. Marinescu I, Axinte DA (2008) A critical analysis of effectiveness of acoustic emission signals to detect tool and workpiece malfunctions in milling operations. Int J Mach Tool Manu 48(10):1148–1160
17. Marinescu I, Axinte D (2009) A time–frequency acoustic emission-based monitoring technique to identify workpiece surface malfunctions in milling with multiple teeth cutting simultaneously. Int J Mach Tool Manu 49(1):53–65
18. Li W, Guo YB, Barkey ME, Jordon JB (2014) Effect tool wear during end milling on the surface integrity and fatigue life of Inconel 718. Procedia CIRP 14:546–551
19. Arunachalam RM, Mannan MA, Spowage AC (2004) Residual stress and surface roughness when facing age hardened Inconel 718 with CBN and ceramic cutting tools. Int J Mach Tool Manu 44(9):879–887
20. Rodriguez A, Laio A (2014) Machine learning. Clustering by fast search and find of density peaks. Science 344(6191):1492–1496
21. Wu M, Schölkopf B, (2007) A local learning approach for clustering. In: Schölkopf B, Platt J, Hofmann T (eds) Advances in neural information processing systems 19 (NIPS 2006). Vancouver 1:1529–1536